

Top-Down Semantic Refinement for Image Captioning

Jusheng Zhang¹, Kaitong Cai¹, Jing Yang¹, Jian Wang¹, Chengpei Tang¹, Keze Wang^{1*}

¹Sun Yat-sen University

Abstract

Large Vision-Language Models (VLMs) face an inherent contradiction in image captioning: their powerful single-step generation capabilities often lead to a **myopic** decision-making process. This makes it difficult to maintain global narrative coherence while capturing rich details, a limitation that is particularly pronounced in tasks that require multi-step and complex scene description. To overcome this fundamental challenge, we redefine image captioning as a **goal-oriented hierarchical refinement planning problem**, and further propose a novel framework, named Top-Down Semantic Refinement (TDSR), which models the generation process as a Markov Decision Process (MDP). However, planning within the vast state space of a VLM presents a significant computational hurdle. Our core contribution, therefore, is the design of a **highly efficient Monte Carlo Tree Search (MCTS) algorithm tailored for VLMs**. By incorporating a **visual-guided parallel expansion** and a **lightweight value network**, our TDSR reduces the call frequency to the expensive VLM by an order of magnitude without sacrificing planning quality. Furthermore, an adaptive early stopping mechanism dynamically matches computational overhead to the image’s complexity. Extensive experiments on multiple benchmarks, including DetailCaps, COMPOSITION-CAP, and POPE, demonstrate that our TDSR, as a plug-and-play module, can significantly enhance the performance of existing VLMs (e.g., LLaVA-1.5, Qwen2.5-VL) by achieving state-of-the-art or highly competitive results in fine-grained description, compositional generalization, and hallucination suppression.

Introduction

At the intersection of computer vision and natural language processing, Large Vision-Language Models (VLMs)(Radford et al. 2021; Jia et al. 2021; Li et al. 2019; Tan and Bansal 2019; Chen et al. 2023a; Vaswani et al. 2017; Chen et al. 2025; Ma et al. 2022; Zhang et al. 2026b) have become the dominant force in image captioning. Through powerful visual encoders and language decoders, these models can generate fluent text that is generally aligned with the image content(Li et al. 2022, 2023a; Wang et al. 2022; Radford et al. 2021; Zhang et al. 2025b). However, despite

their remarkable success, the core auto-regressive generation mechanism of VLMs exposes a fundamental flaw, i.e., an inherent lack of planning capability. When generating each token, VLMs typically employ greedy or beam search strategies(Brown et al. 2020; Hou et al. 2025; Meister, Vieira, and Cotterell 2021; Radford et al. 2019; Rennie et al. 2017; Zhang et al. 2025f). This decision-making process is inherently “myopic”, confined to maximizing local probabilities without “deliberate thought” or foresight and planning capability for the global narrative structure.

This lack of planning capability leads to an intractable dilemma: the model either produces a coherent but detail-poor “safe” description to ensure consistency, or it generates factual errors and logical breaks, i.e., the “hallucination” phenomenon, when attempting to capture rich details without global guidance (Jia et al. 2021; Radford et al. 2021; Rohrbach et al. 2019; OpenAI 2023; Zhang et al. 2025e; Li, Zhang, and Safara 2021). To address this challenge, the research community once turned to a seemingly intuitive “bottom-up” paradigm(Anderson et al. 2018; Yang et al. 2017; Zhang et al. 2021; Stefanini et al. 2021; Herdade et al. 2020). These methods first detect independent regions in an image, describe them separately, and finally “stitch” these fragmented descriptions into a complete caption. However, this “local-to-global” strategy fails to address the core problem. Lacking a unified global plan as an anchor from the outset, the resulting descriptions often degenerate into a simple list of facts, leading to semantic fragmentation and logical incoherence(Rohrbach et al. 2019; Alikhani et al. 2020; Bugliarello and Elliott 2021; Zohourianshahzadi and Kalita 2021; Zhang et al. 2025g). This proves that merely stitching details together cannot effectively compensate for the VLM’s lack of planning ability.

We argue that the root of the problem lies in the generation paradigm itself, and the solution is to fundamentally reframe image captioning as a planning problem. To this end, we propose an innovative “top-down” semantic refinement framework (TDSR), which redefines the task from a unidirectional generation process into a coarse-to-fine, goal-oriented, hierarchical planning process(Yao et al. 2019; Yarats and Lewis 2018; Zhang et al. 2025i). This idea, illustrated in Figure 1, mimics the human cognitive process(Marr 1982; Bar and Bubic 2013; Mefford et al. 2023): first, form a holistic impression of the image to generate a high-level, core descrip-

*Corresponding Author

tion as a “planning blueprint” (e.g., for a picture of people playing cards, an initial description might be “a group of people are sitting in a room doing something”). Then, using this blueprint as a guide, purposefully and progressively explore and fill in key details (e.g., further specifying it as “a group of men are sitting around a table, engaged in a game of Texas Hold’em poker,” and adding that “on the green felt tabletop lie three community cards and a collection of poker chips”). This “global guidance, local refinement” mechanism ensures that all details serve a unified narrative goal, fundamentally guaranteeing high coherence and richness in the description.

Translating this elegant planning concept into an effective computational process hinges on efficient search and planning within the vast language space (Hoang, Haffari, and Cohn 2017; Wiher, Meister, and Cotterell 2022). We rigorously formalize this process as a Markov Decision Process (MDP (Puterman 1994)) and employ Monte Carlo Tree Search (MCTS (Świechowski et al. 2022; Kemmerling, Lütticke, and Schmitt 2023)) as the core engine. However, directly applying standard MCTS to a VLM is computationally infeasible due to the model’s massive inference cost (Browne et al. 2012a). Therefore, our core technical contribution lies in deeply optimizing the MCTS algorithm to enable efficient planning within VLMs. By incorporating a Visual-Guided Parallel Expansion mechanism and a lightweight value network, our algorithm reduces the call frequency to the expensive VLM by an order of magnitude without sacrificing planning quality, successfully resolving the efficiency bottleneck. Our framework (TDSR), as a plug-and-play module, significantly enhances the performance of existing VLMs and achieves state-of-the-art or highly competitive results on multiple benchmarks.

Our core contributions can be summarized in three points:

- **A Novel “Planning-based” Generation Paradigm:** We propose a “Top-Down” planning framework (TDSR) that redefines image captioning as a coarse-to-fine hierarchical planning problem. This fundamentally resolves the “myopic” flaw of traditional generative models, ensuring both global narrative coherence and local detail richness.
- **An Efficient MCTS Algorithm Tailored for VLMs:** We design a highly efficient Monte Carlo Tree Search (MCTS) algorithm to address the high inference cost of VLMs. The algorithm broadens search breadth via a “Visual-Guided Parallel Expansion” mechanism and uses a “lightweight value network” for fast value estimation, reducing the call frequency to the expensive VLM by an order of magnitude without sacrificing planning quality.
- **A Dynamic and Adaptive Search Control Strategy:** We introduce a dynamic control strategy to enhance planning efficiency and quality. The strategy guides the search direction through a composite reward function combining a “redundancy penalty” and a “depth incentive,” and it intelligently allocates computational resources based on image complexity via an “adaptive early stopping” mechanism to avoid unnecessary overhead.

Related Work

Early Encoder-Decoder Architectures

As a cross-disciplinary field between computer vision and natural language processing (Zhang et al. 2025c; Radford et al. 2021; Jia et al. 2021; Chen et al. 2023a; Zhang et al. 2025a, 2026c), early research in image captioning primarily adopted the encoder-decoder framework. Methods represented by Show and Tell (Vinyals et al. 2015; Zhang et al. 2025d,h) used a CNN (Krizhevsky, Sutskever, and Hinton 2012; Lecun et al. 1998; Ma et al. 2024a,b, 2025e,d) to extract global image features and an RNN (Elman 1990; Ma et al. 2025a,b,c; Shen et al. 2025; Long et al. 2025) to generate a fluent description. Subsequently, Show, Attend and Tell (Vinyals et al. 2015) introduced an attention mechanism, allowing the model to focus on local regions of the image. These pioneering works excelled at generating grammatically coherent sentences, but their mechanism of generating a single, holistic description meant they often overlooked fine-grained object details, leading to a lack of richness and specificity. **This is precisely one of the core problems our TDSR framework aims to solve through multi-step refinement.**

The “Bottom-up” Generation Paradigm

To enhance detail capture, subsequent research shifted towards the “bottom-up” paradigm (Anderson et al. 2018; Yang et al. 2017; Zhang et al. 2021; Stefanini et al. 2021; Herdade et al. 2020). This approach typically first identifies independent objects or regions in an image, generates local descriptions for them, and finally stitches these segments into a complete sentence. DenseCap (Johnson, Karpathy, and Fei-Fei 2015) is a typical representative of this line of work, which utilizes an object detector to locate and describe regions individually. Follow-up works, such as Patch Matters (Peng et al. 2025b; Zhang et al. 2026d,a) and FineCaption (Hua et al. 2024b), focused on improving the quality of these local descriptions. Although these methods significantly increased detail richness, their “split-first, stitch-later” process inherently decouples from the global context, often leading to semantic fragmentation and insufficient global coherence. In stark contrast, our “top-down” approach, guided by global context, fundamentally avoids the inconsistency issues inherent in the “split-first, stitch-later” process.

Large Vision-Language Models and Generation Refinement Strategies

In recent years, Large Vision-Language Models (VLMs), such as LLaVA-1.5 (Liu et al. 2023b), Qwen-VL (Bai, Bai, and et al. 2023), and Ferret (You and et al. 2023), have significantly advanced visual narrative capabilities through pre-training on massive image-text data. However, despite their powerful foundational abilities, their standard autoregressive generation still faces the inherent trade-off between detail and coherence. Consequently, several training-free enhancement methods have emerged. For instance, some works employ iterative prompting (e.g., IT (Zhou et al. 2023)) to induce the model to output more details.

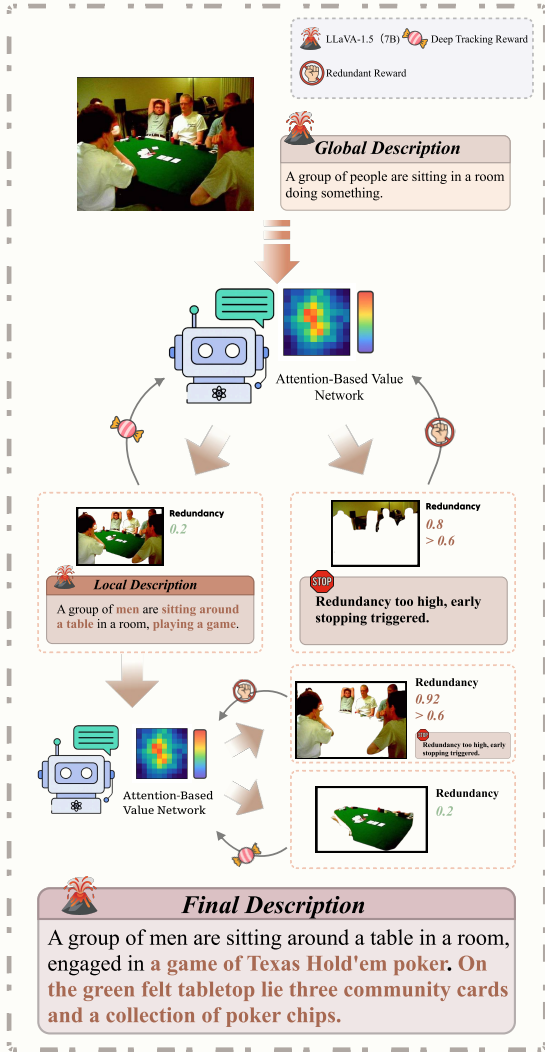


Figure 1: The TDSR framework generates coherent, detailed captions through global-to-local refinement, guided by redundancy-aware stopping and efficient MCTS.

A more promising direction involves formalizing the generation process as a search problem and employing planning algorithms like Monte Carlo Tree Search (MCTS) for optimization (Browne et al. 2012b; Yao et al. 2023; Silver et al. 2017). Against this backdrop, our TDSR framework proposes a more fundamental solution. It also employs MCTS, but its core innovation lies in how to tailor and efficiently execute the search for VLMs. Our method is guided by a sophisticated composite reward function and integrates a suite of efficiency optimization mechanisms, including visual-guided parallel rollouts and dynamic redundancy control. **Consequently, TDSR is not only superior in its paradigm ('top-down') but also innovative in its solution strategy (efficient MCTS), thereby efficiently uni-**

fyng detail and coherence while significantly mitigating issues like semantic fragmentation and content hallucination.

Method

This section details our Top-Down Semantic Refinement (TDSR) framework. We begin by formalizing the task of progressive image description as a Markov Decision Process (MDP), explicitly framing it as a planning problem. We then present our core contribution: a highly efficient Monte Carlo Tree Search (MCTS) (Kocsis and Szepesvári 2006; Browne et al. 2012b; Yao et al. 2023) algorithm designed to solve this MDP. Our MCTS variant introduces several key optimizations, including a **Visual-Guided Parallel Expansion** strategy, a **lightweight value network** for fast simulations, and dynamic reward shaping, which collectively enable high-quality planning without incurring prohibitive computational costs.

Image Captioning as a Planning Problem

We cast the challenge of generating a detailed and coherent caption $Y = (y_1, y_2, \dots, y_L)$ for an image I as a sequential decision-making problem. The goal is to find an optimal policy π^* that generates a sequence of tokens maximizing a cumulative reward. This process is formally defined as a Markov Decision Process (MDP), specified by the tuple $(\mathcal{S}, \mathcal{A}, \mathcal{P}, \mathcal{R})$:

State \mathcal{S} : A state $s_t \in \mathcal{S}$ is the prefix of a caption being generated, represented by the sequence of tokens (y_1, \dots, y_t) . The initial state s_0 can be an empty sequence or a high-level caption generated by a base VLM.

Action \mathcal{A} : An action $a_t \in \mathcal{A}$ corresponds to selecting the next token y_{t+1} to append to the current sequence. The set of possible actions is the model's vocabulary.

Transition \mathcal{P} : The transition function $\mathcal{P}(s_{t+1}|s_t, a_t)$ is deterministic: taking action a_t in state s_t leads to state $s_{t+1} = s_t \oplus a_t$, where \oplus denotes concatenation.

Reward \mathcal{R} : Upon reaching a terminal state s_T (e.g., by generating an end-of-sequence token), the environment returns a terminal reward $R(s_T)$. This reward function is meticulously designed to encourage detailed, coherent, and non-repetitive descriptions:

$$R(s_T) = R_{\text{quality}}(s_T, I) + R_{\text{depth}}(s_T) - P_{\text{redundancy}}(s_T) \quad (1)$$

where R_{quality} assesses fine-grained relevance and compositional correctness (e.g., using CLIP-based scores). The term $R_{\text{depth}} = \alpha \cdot \log(1 + |s_T|)$ provides a **depth incentive** to encourage longer, more detailed descriptions. Finally, $P_{\text{redundancy}}$ penalizes semantic repetition using efficient metrics like n-gram overlap.

The objective is to find a policy $\pi(a_t|s_t)$ that maximizes the expected reward. Given the massive state-action space, we employ MCTS as a powerful online planning algorithm to approximate the optimal policy.

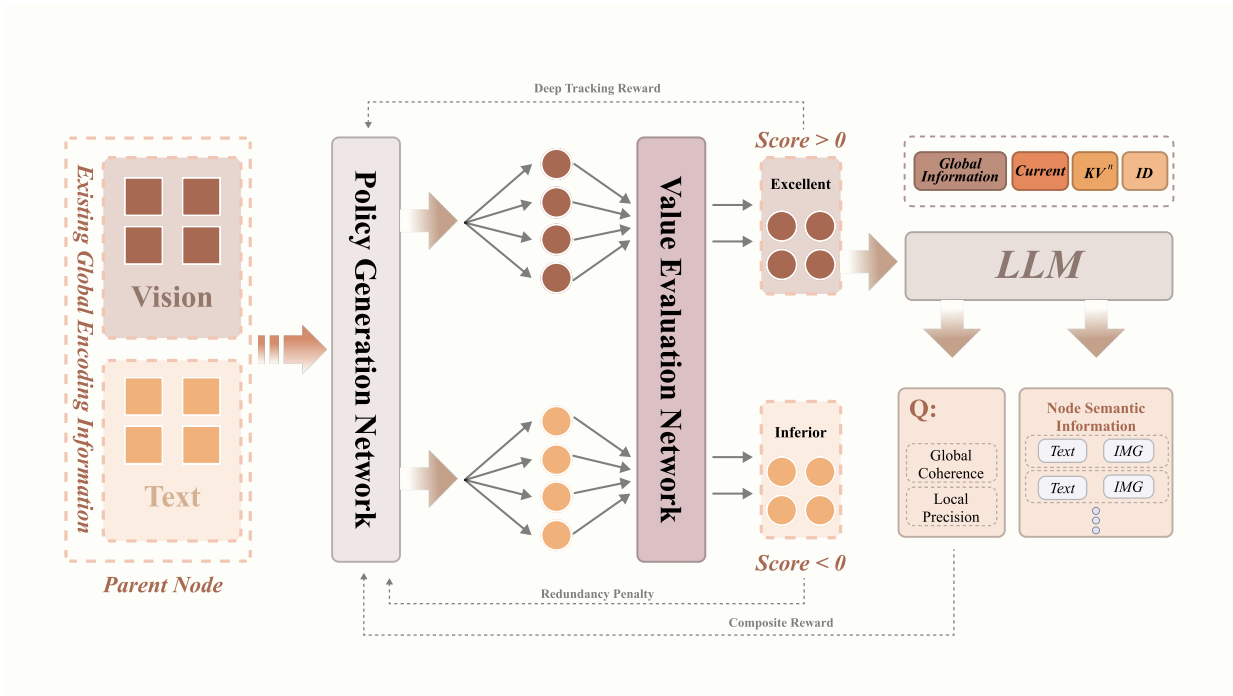


Figure 2: The architecture of TDSR’s MCTS planner. The four canonical stages, i.e., selection, visual-guided parallel expansion, lightweight value estimation, and backpropagation, are tailored to efficiently search within VLMs. Composite rewards combine local precision and global coherence.

MCTS for Coarse-to-Fine Planning

MCTS is an ideal choice for this problem as it builds a search tree asynchronously (Yao et al. 2023), focusing its computational efforts on more promising regions of the state space. Our key innovation lies in how we integrate the VLM and other components into the four canonical steps of MCTS. The entire TDSR process is outlined in Algorithm 1.

At any node s in the search tree, we store the total action value $W(s, a)$, the visit count $N(s, a)$, and the prior probability $P(s, a)$ for each action a .

1. Selection. Starting from the root node, we recursively select the action that maximizes the Upper Confidence Bound for Trees (UCT) criterion until a leaf node s_L is reached. The summation in the UCT formula is over all valid actions b from state s_t :

$$a_t = \arg \max_a \left(Q(s_t, a) + c_{\text{puct}} \cdot P(s_t, a) \cdot \frac{\sqrt{\sum_b N(s_t, b)}}{1 + N(s_t, a)} \right) \quad (2)$$

Here, $Q(s, a) = W(s, a)/N(s, a)$ is the mean action value (exploitation term), and $P(s, a)$ is the **policy prior** derived from our base VLM to guide the search.

Visual-Guided Parallel Expansion. Upon reaching a leaf node s_L , instead of expanding only one path, we guide the VLM to explore multiple, visually-grounded semantic paths in parallel. This unfolds in two stages:

1. Salient Region Identification: We leverage cross-attention maps from the VLM \mathcal{G}_θ or an external object

detector to identify k salient image regions not yet adequately described in the current caption s_L .

2. Parallel Prompting and Expansion: For each region, we construct a unique exploratory prompt (e.g., “Describe the person’s clothing in more detail.”). We then execute the VLM \mathcal{G}_θ in parallel for these k inputs. This single batch-forward pass yields k policy vectors and k VLM-based value estimates:

$$(p_a^{(i)}, v_{\text{vlm}}^{(i)}) = \mathcal{G}_\theta(\text{prompt}_i, s_L, I) \quad \text{for } i = 1, \dots, k \quad (3)$$

The node s_L is then expanded with new children corresponding to promising actions from the policy vectors $p_a^{(i)}$. This ensures search breadth is explicitly grounded in diverse visual evidence.

Simulation (and Lightweight Value Estimation). This step is critical for efficiency. Instead of performing a costly “rollout” with the VLM, we estimate the value of the new leaf node s_L using a separate, **lightweight value network** \mathcal{V}_ϕ . This network is trained to approximate the final reward $R(s_T)$ from an intermediate state:

$$\hat{v} = \mathcal{V}_\phi(s_L, I) \quad (4)$$

This AlphaGo-inspired approach replaces expensive simulations with a single, fast forward pass. The final value estimate V is a weighted combination of the VLM’s coarse estimate from the expansion step (v_{vlm}) and the specialized value network’s estimate (\hat{v}):

$$V = \lambda_v \cdot v_{\text{vlm}} + (1 - \lambda_v) \cdot \hat{v} \quad (5)$$

Algorithm 1: Top-Down Semantic Refinement (TDSR)

```
1: function TDSR_GENERATE( $I, L$ )
2:    $s_{\text{caption}} \leftarrow$  initial prompt or empty sequence
3:   for  $t = 1$  to  $L$  do
4:      $s_{\text{root}} \leftarrow s_{\text{caption}}$ 
5:     Initialize MCTS tree  $T$  with root node  $s_{\text{root}}$ 
6:     for  $i = 1$  to  $N_{\text{max\_iterations}}$  do
7:        $s_{\text{leaf}} \leftarrow$  SelectLeafNode( $s_{\text{root}}, T$ )
8:        $(P, v_{\text{vlm}}) \leftarrow$  Expand( $s_{\text{leaf}}, I$ )  $\triangleright$  Via
       visual-guided parallel expansion
9:        $\hat{v} \leftarrow \mathcal{V}_{\phi}(s_{\text{leaf}}, I)$   $\triangleright$  Estimate value with
       lightweight network
10:       $V \leftarrow \lambda_v \cdot v_{\text{vlm}} + (1 - \lambda_v) \cdot \hat{v}$   $\triangleright$  Combine
       value estimates
11:      Backpropagate value  $V$  from  $s_{\text{leaf}}$  to  $s_{\text{root}}$ 
12:      if search has converged at root then  $\triangleright$ 
       Adaptive termination
13:        break
14:      end if
15:    end for
16:     $y_{t+1} \leftarrow \arg \max_a N(s_{\text{root}}, a)$   $\triangleright$  Select best
       action
17:    if  $y_{t+1}$  is end-of-sequence token then
18:      break
19:    end if
20:     $s_{\text{caption}} \leftarrow s_{\text{caption}} \oplus y_{t+1}$ 
21:  end for
22:  return  $s_{\text{caption}}$ 
23: end function
```

Value Network Architecture and Training. The lightweight value network \mathcal{V}_{ϕ} is designed for speed. Its architecture consists of a 4-layer Transformer encoder that processes the token sequence s_L , whose output is then concatenated with the global image features from the VLM’s vision encoder. This combined representation is passed through a 2-layer MLP head to regress a single scalar value \hat{v} . To train \mathcal{V}_{ϕ} , we generate a dataset of state-reward pairs by running the full TDSR search on a large corpus of images. For each completed search, we store all intermediate states s_t encountered and the final, true reward $R(s_T)$ of the resulting caption. The network is then trained offline using a Mean Squared Error (MSE) loss between its prediction \hat{v} for a state s_t and the corresponding ground-truth terminal reward $R(s_T)$. **Backpropagation.** The combined value estimate V is propagated back up the tree to update the visit counts $N(s, a)$ and total action values $W(s, a)$ for all edges on the traversed path from s_L to the root. **Pragmatic Implementation: Adaptive Termination.** To further optimize efficiency, the number of MCTS iterations ($N_{\text{max_iterations}}$) is not fixed. We employ an **adaptive early stopping** mechanism. The search is terminated when the UCT value of the best root action shows negligible improvement over several iterations, indicating convergence.

Experiment

Experimental Settings

Evaluation Tasks In this study, we evaluate the performance of our method on three distinct and comprehensive benchmark datasets: **DetailCaps**(Dong et al. 2024), **COMPOSITIONCAP**(Hua et al. 2024a), and **POPE**(Li et al. 2023b), each of which aims to assess different aspects of image description and reasoning tasks. **DetailCaps:** This benchmark provides a high-quality image captioning dataset to evaluate LVLMs on their ability to generate detailed descriptions at the object, attribute, and relationship levels. The **CAPTURE metric** measures detail coverage across these dimensions, offering a systematic framework for assessing multimodal models’ fine-grained image understanding. **COMPOSITIONCAP:** This benchmark evaluates the compositional generalization ability of multimodal models, focusing on their capacity to describe images with novel combinations of objects, attributes, and relationships. It tests models’ compositional reasoning by requiring accurate descriptions of unseen combinations. **POPE:** This benchmark is designed to assess the phenomenon of object hallucination in multimodal large models. It focuses on detecting whether models falsely “fabricate” objects or details that do not exist in the image during image description or question-answering tasks.

Baselines To systematically evaluate the generalization and practical effectiveness of **TDSR** across different model architectures, we deploy it on two widely adopted multimodal large language models: **Qwen2.5-VL**(Bai et al. 2025) and **LLaVA-1.5 (7B)**(Liu et al. 2023a). We compare it against a diverse set of representative baselines, which fall into two major paradigms: **Training-free image captioning enhancement methods:** including *IT*(Pi et al. 2024), *Patch Matters*(Peng et al. 2025a), and *FINECAPTION*, which improve visual description quality without additional training. All baselines in this category are implemented on top of LLaVA-1.5 (7B). **Foundation vision-language models:** including *Shikra-13B*(Chen et al. 2023c), *MiniGPT-v2*(Chen et al. 2023b), *Ferret-13B*(You et al. 2023), *VisionLLM-H*(Wang et al. 2023), *KOSMOS-2*(Peng et al. 2023), *Alpha-CLIP-13B*(Sun et al. 2023), and *VistaLLM*(Pramanick et al. 2023), representing the dominant modeling paradigms in the open-source multimodal field.

Implementation Details Our TDSR framework is implemented in PyTorch. For the core MCTS algorithm, we set the UCT exploration constant c_{puct} to 1.5. The reward depth incentive weight α is set to 0.1. During inference, we applied TDSR to refine the outputs of both Qwen2.5-VL and LLaVA-1.5 (7B). **A comprehensive list of all hyperparameters, including the value network architecture and training specifics, is provided in Appendix A for reproducibility.**

Benchmark Model Comparison Experiment

DetailCaps Result The experimental results presented in Table 1 on the DETAILCAPS benchmark demonstrate that **TDSR** significantly enhances fine-grained semantic

Table 1: Performance comparison on the DetailCaps benchmark. TDSR-enhanced models achieve consistent improvements across all fine-grained metrics.

Method	CAPTURE	F1_obj	F1_attr	F1_rel
Shikra-13B	60.5	61.9	55.4	56.4
MiniGPT-v2-7B	61.2	62.7	55.9	56.8
Ferret-13B	62.8	63.2	56.4	57.3
VisionLLM-H-7B	57.9	59.3	53.4	53.9
KOSMOS-2	58.5	60.8	53.1	54.2
Alpha-CLIP-13B	59.2	61.9	57.2	56.5
FINECAPTION-8B	63.4	63.7	58.1	58.3
VistaLLM-13B	63.2	63.5	60.3	59.2
LLaVA-1.5-7B+IT	51.98	56.3	48.2	50.4
LLaVA-1.5-7B+Patch Matters	58.05	62.2	56.1	52.5
LLaVA-1.5-7B	49.99	55.7	44.4	49.4
LLaVA-1.5-7B+ours	66.7	66.2	62.4	63.4
Qwen2.5-VL-7B	64.7	66.7	62.5	62.3
Qwen2.5-VL-7B+ours	72.2	72.3	65.2	64.7

Table 2: Benchmark comparison on the COMPOSITION-CAP dataset. Our method significantly outperforms all baselines across all metrics.

Method	ROUGE-L↑	BLEU-4↑	METEOR↑	CIDEr↑	BERT Score↑
Shikra-13B	32.4	11.9	19.5	108.4	78.4
MiniGPT-v2-7B	31.9	11.5	18.7	106.2	78.2
Ferret-13B	33.6	12.8	19.6	114.6	79.1
VisionLLM-H-7B	31.2	10.7	15.4	90.2	76.5
KOSMOS-2	30.8	10.1	14.9	88.9	76.7
Alpha-CLIP-13B	35.6	10.9	19.3	93.9	77.7
FINECAPTION-8B	40.6	13.9	20.9	118.6	79.5
VistaLLM-13B	40.9	14.1	21.4	117.5	80.2
LLaVA-1.5-7B+IT	32.9	10.6	15.7	95.2	78.2
LLaVA-1.5-7B+Patch Matters	34.6	12.5	21.2	118.8	79.1
LLaVA-1.5-7B	30.3	8.6	11.4	86.5	73.2
LLaVA-1.5-7B+ours	44.3	16.6	23.5	124.2	82.5
Qwen2.5-VL-7B	41.2	14.5	21.9	120.3	81.3
Qwen2.5-VL-7B+ours	47.5	19.7	27.5	129.4	88.9

understanding in multimodal models, particularly in object, attribute, and relation-level comprehension. Under the LLaVA architecture, LLaVA-1.5+OURS exhibits notable improvements across all three fine-grained metrics ($F1_{obj}$, $F1_{attr}$, $F1_{rel}$) compared to the base model. In particular, $F1_{attr}$ rises markedly from 44.4 to 62.4, validating the effectiveness of TDSR in capturing detailed semantic signals in image descriptions. Within the stronger QWEN2.5-VL architecture, TDSR further advances overall performance, achieving a CAPTURE score of 72.2, with $F1_{obj}$ and $F1_{rel}$ reaching 72.3 and 64.7 respectively, both significantly outperforming all other baselines. These results highlight the robust semantic modeling and visual-linguistic alignment capacity brought by TDSR. The proposed semantics-driven exploration mechanism exhibits consistent and effective improvements across both architectures, markedly enhancing the model’s ability to capture key semantic units from images.

COMPOSITIONCAP Result The experimental results presented in Table 2 on the COMPOSITIONCAP benchmark demonstrate the effectiveness of the proposed TDSR method across different vision-language model architectures. Within the LLaVA framework, the incorporation of TDSR (LLaVA-1.5+ours) consistently improves perfor-

mance over the base model, with ROUGE-L increasing to 44.3 and CIDEr reaching 124.2, indicating enhanced descriptive completeness and detail sensitivity. In the stronger Qwen2.5-VL framework, TDSR yields further performance gains, achieving a CIDEr of 129.4 and a BERTScore of 88.9 (the best results to date), highlighting its superior modeling of visual-semantic consistency and linguistic precision.

Overall, compared to traditional non-trained augmentation methods (e.g., *IT*, *Patch Matters*, *FINECAPTION*) and mainstream multimodal models (e.g., *Ferret*, *VistaLLM*, *KOSMOS-2*), TDSR consistently demonstrates strong capabilities in cross-modal reasoning, compositional understanding, and expressive generation under both Qwen and LLaVA backbones.

Hallucination Evaluation

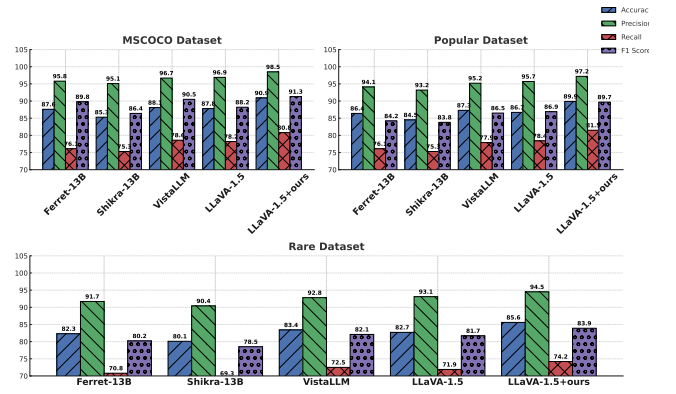


Figure 3: POPE benchmark results. TDSR improves hallucination robustness across random, popular, and adversarial settings.

As shown in Figure 3, we conduct a systematic evaluation of several state-of-the-art multimodal models on the POPE benchmark, which is designed to assess hallucination robustness under three types of semantic perturbations: **Random**, **Popular**, and **Adversarial**. POPE explicitly tests whether a model hallucinates non-existent entities or attributes in response to misleading prompts. Results indicate that LLaVA-1.5+TDSR consistently achieves the best performance across all settings, demonstrating superior robustness. Notably, under the most challenging **Adversarial** condition, it maintains an Accuracy of 86.3 and an F1 Score of 84.3, significantly outperforming other models. In the relatively simpler **Random** setting, it achieves the highest F1 Score of 91.3, slightly ahead of VistaLLM (90.5). In the more ambiguous **Popular** setting, where semantically frequent entities such as “person” or “cat” may induce biased responses, most models experience a notable performance drop, i.e., Ferret-13B and Shikra-13B fall to 84.2 and 83.8 respectively, while LLaVA-1.5+TDSR remains stable at 87.1, highlighting its robustness and generalization to biased prompts.

We attribute TDSR’s resistance to hallucination to its **top-down semantic reasoning**: a strong global context steers

attention to the truly relevant regions when parsing fine-grained objects, thereby minimizing misalignment and fabricated details.

Efficiency Analysis

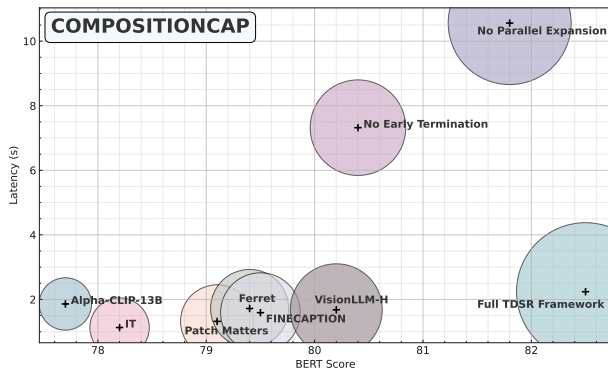


Figure 4: Efficiency-performance tradeoff of TDSR. The full framework achieves the best generation quality (BERTScore) with only a marginal latency increase, clearly outperforming prior methods.

To comprehensively assess the efficiency-performance tradeoff of the TDSR framework, we conduct a series of controlled experiments comparing the full TDSR architecture, its variants with individual efficiency components disabled, and several representative vision-language baselines. The evaluation focuses on two primary metrics: inference latency and generation quality (measured by **BERTScore**).

As shown in Figure 4, the full TDSR framework achieves strong generation performance while maintaining a reasonable inference delay. Specifically, although its average latency slightly increases to **2.24s/frame**, this overhead remains marginal compared to mainstream baselines such as *VisionLLM-H* (1.68s), *FINECAPTION* (1.59s), and *Ferret* (1.72s). In contrast, TDSR yields a substantial improvement in output quality, achieving the highest **BERTScore of 82.5** on the *COMPOSITIONCAP* benchmark, significantly outperforming the aforementioned models (e.g., *Ferret*: 79.4, *FINECAPTION*: 79.5, *VisionLLM-H*: 80.2). The efficiency of TDSR is largely attributed to the incorporation of parallel expansion and early termination strategies. Without parallel expansion, the latency sharply rises to **10.56s**, i.e., a **4.71x** increase. Similarly, disabling early termination incurs an additional **5.08s** of delay, alongside a noticeable degradation in output quality.

Ablation studies

To assess the contribution of each TDSR component, we randomly sample **100 COCO images** and track step-wise **CIDEr** and **BLEU-4** scores across 10 exploration steps. The ablation variants are: **w/o value estimation**: Disable value network; select regions randomly without semantic lookahead; **w/o redundancy penalty**: Remove penalties on repeated or overlapping descriptions; **w/o depth-aware reward**: Drop the reward term for fine-grained region track-

ing; **w/o early termination**: Always run 10 steps regardless of confidence; **Full TDSR**: All modules enabled as the default configuration. The ablation results (Fig. 5–6)

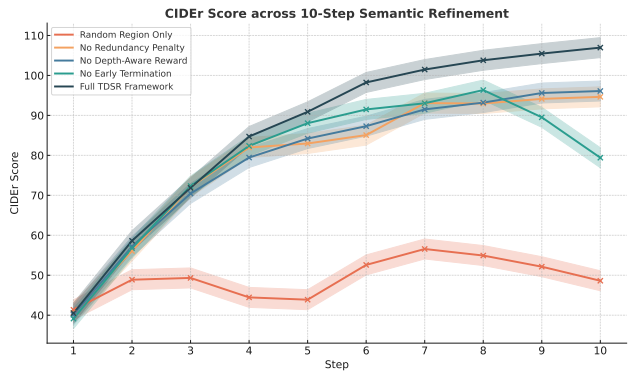


Figure 5: Step-wise CIDEr score under ablation settings. Removing any core component from TDSR results in significant performance drops, especially in early stopping and value-guided region selection.

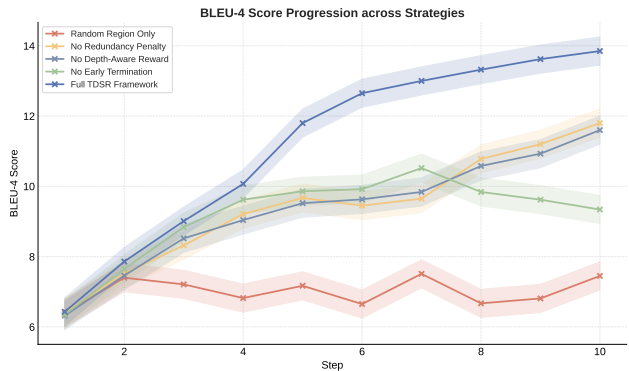


Figure 6: Step-wise BLEU-4 score under ablation settings. Full TDSR achieves the highest and most stable performance; removing value estimation or early stopping severely degrades output fluency.

show that the five modules of TDSR are complementary and non-redundant. **Value-guided region selection.** Disabling it (*Random Region Only*) causes the steepest decline, as the planner no longer attends to salient areas, dropping scores to CIDEr 48.62, and BLEU-4 7.45. **Redundancy penalty & depth-aware reward.** Removing either one slows convergence and yields repetitive or shallow sentences, with final scores stalled around CIDEr 94.64/96.10 and BLEU-4 11.8/11.6. **Early termination.** When always running the full 10 steps, the model initially rivals the complete framework but then over-generates, causing CIDEr to fall from 96.34 to 79.41 and BLEU-4 to 9.34. These drops underline that each component is essential for maintaining both descriptiveness and coherence.

Conclusion

We propose **TDSR**, a top-down semantic-refinement framework that reformulates image captioning as a coarse-to-fine planning task. Driven by an MCTS planner, TDSR first drafts a global caption and then incrementally enriches it with visually grounded details. Three key techniques, i.e., (i) a lightweight value network, (ii) redundancy-aware early stopping, and (iii) adaptive rollout depth, jointly deliver high caption quality at modest computational cost. Across detail, compositionality, and hallucination benchmarks, TDSR consistently raises factual accuracy, descriptive richness, and robustness to visual perturbations. Ablation experiments show that removing any one component leads to sizable drops in CIDER and BLEU-4, underscoring their complementarity.

References

- Alikhani, M.; Sharma, P.; Li, S.; Soricut, R.; and Stone, M. 2020. Cross-modal Coherence Modeling for Caption Generation. In *Proceedings of the 58th Annual Meeting of the Association for Computational Linguistics*, 6525–6535. Association for Computational Linguistics.
- Anderson, P.; He, X.; Buehler, C.; Teney, D.; Johnson, M.; Gould, S.; and Zhang, L. 2018. Bottom-Up and Top-Down Attention for Image Captioning and Visual Question Answering. *arXiv:1707.07998*.
- Bai, J.; Bai, S.; and et al. 2023. Qwen-VL: A Versatile Vision-Language Model for Understanding, Localization, Text Reading, and Beyond. *arXiv:2308.12966*.
- Bai, S.; Chen, K.; Liu, X.; Wang, J.; Ge, W.; Song, S.; Dang, K.; Wang, P.; Wang, S.; Tang, J.; Zhong, H.; Zhu, Y.; Yang, M.; Li, Z.; Wan, J.; Wang, P.; Ding, W.; Fu, Z.; Xu, Y.; Ye, J.; Zhang, X.; Xie, T.; Cheng, Z.; Zhang, H.; Yang, Z.; Xu, H.; and Lin, J. 2025. Qwen2.5-VL Technical Report. *arXiv preprint arXiv:2502.13923*.
- Bar, M.; and Bubic, A. 2013. Top-Down Effects in Visual Perception. In Ochsner, K. N.; and Kosslyn, S. M., eds., *The Oxford Handbook of Cognitive Neuroscience*, volume 1 of *The Oxford Handbook Series*, 60–73. Oxford University Press.
- Brown, T. B.; Mann, B.; Ryder, N.; Subbiah, M.; Kaplan, J.; Dhariwal, P.; Neelakantan, A.; Shyam, P.; Sastry, G.; Askell, A.; Agarwal, S.; Herbert-Voss, A.; Krueger, G.; Henighan, T.; Child, R.; Ramesh, A.; Ziegler, D. M.; Wu, J.; Winter, C.; Hesse, C.; Chen, M.; Sigler, E.; Litwin, M.; Gray, S.; Chess, B.; Clark, J.; Berner, C.; McCandlish, S.; Radford, A.; Sutskever, I.; and Amodei, D. 2020. Language Models are Few-Shot Learners. *arXiv:2005.14165*.
- Browne, C. B.; Powley, E.; Whitehouse, D.; Lucas, S. M.; Cowling, P. I.; Rohlfshagen, P.; Tavener, S.; Perez, D.; Samothrakis, S.; and Colton, S. 2012a. A Survey of Monte Carlo Tree Search Methods. *IEEE Transactions on Computational Intelligence and AI in Games*, 4(1): 1–43.
- Browne, C. B.; Powley, E.; Whitehouse, D.; Lucas, S. M.; Cowling, P. I.; Rohlfshagen, P.; Tavener, S.; Perez, D.; Samothrakis, S.; and Colton, S. 2012b. A Survey of Monte Carlo Tree Search Methods. *IEEE Transactions on Computational Intelligence and AI in Games*, 4(1): 1–43.
- Bugliarello, E.; and Elliott, D. 2021. The Role of Syntactic Planning in Compositional Image Captioning. *arXiv:2101.11911*.
- Chen, F.-L.; Zhang, D.-Z.; Han, M.-L.; Chen, X.-Y.; Shi, J.; Xu, S.; and Xu, B. 2023a. VLP: A Survey on Vision-language Pre-training. *Machine Intelligence Research*, 20(1): 38–56.
- Chen, J.; Zhu, D.; Shen, X.; Li, X.; Liu, Z.; Zhang, P.; Krishnamoorthi, R.; Chandra, V.; Xiong, Y.; and Elhoseiny, M. 2023b. MiniGPT-v2: Large Language Model as a Unified Interface for Vision-Language Multi-task Learning. *arXiv:2310.09478*.
- Chen, K.; Zhang, Z.; Zeng, W.; Zhang, R.; Zhu, F.; and Zhao, R. 2023c. Shikra: Unleashing Multimodal LLM’s Referential Dialogue Magic. *arXiv preprint arXiv:2306.15195*.
- Chen, Y.; He, X.; Ma, X.; and Ma, Y. 2025. ContextFlow: Training-Free Video Object Editing via Adaptive Context Enrichment. *arXiv preprint arXiv:2509.17818*.
- Dong, H.; Li, J.; Wu, B.; Wang, J.; Zhang, Y.; and Guo, H. 2024. Benchmarking and Improving Detail Image Caption. *arXiv preprint arXiv:2405.19092*.
- Elman, J. L. 1990. Finding Structure in Time. *Cognitive Science*, 14(2): 179–211.
- Herdade, S.; Kappeler, A.; Boakye, K.; and Soares, J. 2020. Image Captioning: Transforming Objects into Words. *arXiv:1906.05963*.
- Hoang, C. D. V.; Haffari, G.; and Cohn, T. 2017. Towards Decoding as Continuous Optimization in Neural Machine Translation. *arXiv:1701.02854*.
- Hou, Y.; Giledereli, B.; Tu, Y.; and Sachan, M. 2025. Do Vision-Language Models Really Understand Visual Language? In *Forty-second International Conference on Machine Learning*.
- Hua, H.; Liu, Q.; Zhang, L.; Shi, J.; Sooye, K.; Zhang, Z.; Wang, Y.; Zhang, J.; and Luo, J. 2024a. FINECAPTION: Compositional Image Captioning Focusing on Wherever You Want at Any Granularity. *arXiv preprint arXiv:2411.15411*.
- Hua, H.; Liu, Q.; Zhang, L.; Shi, J.; Zhang, Z.; Wang, Y.; Zhang, J.; and Luo, J. 2024b. FINECAPTION: Compositional Image Captioning Focusing on Wherever You Want at Any Granularity. *arXiv:2411.15411*.
- Jia, C.; Yang, Y.; Xia, Y.; Chen, Y.-T.; Parekh, Z.; Pham, H.; Le, Q. V.; Sung, Y.; Li, Z.; and Duerig, T. 2021. Scaling Up Visual and Vision-Language Representation Learning With Noisy Text Supervision. *arXiv:2102.05918*.
- Johnson, J.; Karpathy, A.; and Fei-Fei, L. 2015. DenseCap: Fully Convolutional Localization Networks for Dense Captioning. *arXiv:1511.07571*.
- Kemmerling, M.; Lütticke, D.; and Schmitt, R. H. 2023. Beyond games: a systematic review of neural Monte Carlo tree search applications. *Applied Intelligence*, 54(1): 1020–1046.
- Kocsis, L.; and Szepesvári, C. 2006. Bandit Based Monte-Carlo Planning. In *Proceedings of the 17th European Conference on Machine Learning (ECML)*, 282–293. Springer.

- Krizhevsky, A.; Sutskever, I.; and Hinton, G. E. 2012. ImageNet Classification with Deep Convolutional Neural Networks. In *Advances in Neural Information Processing Systems 25 (NeurIPS 2012)*, 1097–1105.
- Lecun, Y.; Bottou, L.; Bengio, Y.; and Haffner, P. 1998. Gradient-based learning applied to document recognition. *Proceedings of the IEEE*, 86(11): 2278–2324.
- Li, J.; Li, D.; Savarese, S.; and Hoi, S. 2023a. BLIP-2: Bootstrapping Language-Image Pre-training with Frozen Image Encoders and Large Language Models. arXiv:2301.12597.
- Li, J.; Li, D.; Xiong, C.; and Hoi, S. C. 2022. BLIP: Bootstrapping Language-Image Pre-training for Unified Vision-Language Understanding and Generation. In *Proceedings of the 39th International Conference on Machine Learning (ICML)*, volume 162 of *Proceedings of Machine Learning Research*, 12888–12900. PMLR.
- Li, L. H.; Yatskar, M.; Yin, D.; Hsieh, C.-J.; and Chang, K.-W. 2019. VisualBERT: A Simple and Performant Baseline for Vision and Language. arXiv:1908.03557.
- Li, X.; Zhang, J.; and Safara, F. 2021. Improving the Accuracy of Diabetes Diagnosis Applications through a Hybrid Feature Selection Algorithm. *Neural Process. Lett.*, 55(1): 153–169.
- Li, Y.; Du, Y.; Zhou, K.; Wang, J.; Zhao, W. X.; and Wen, J.-R. 2023b. Evaluating Object Hallucination in Large Vision-Language Models. In *The 2023 Conference on Empirical Methods in Natural Language Processing*.
- Liu, H.; Li, C.; Li, Y.; and Lee, Y. J. 2023a. Improved Baselines with Visual Instruction Tuning.
- Liu, H.; Li, C.; Wu, Q.; and Lee, Y. J. 2023b. Visual Instruction Tuning. arXiv:2304.08485.
- Long, Z.; Zheng, M.; Feng, K.; Zhang, X.; Liu, H.; Yang, H.; Zhang, L.; Chen, Q.; and Ma, Y. 2025. Follow-your-shape: Shape-aware image editing via trajectory-guided region control. arXiv preprint arXiv:2508.08134.
- Ma, Y.; Feng, K.; Hu, Z.; Wang, X.; Wang, Y.; Zheng, M.; He, X.; Zhu, C.; Liu, H.; He, Y.; et al. 2025a. Controllable Video Generation: A Survey. arXiv preprint arXiv:2507.16869.
- Ma, Y.; Feng, K.; Zhang, X.; Liu, H.; Zhang, D. J.; Xing, J.; Zhang, Y.; Yang, A.; Wang, Z.; and Chen, Q. 2025b. Follow-Your-Creation: Empowering 4D Creation through Video Inpainting. arXiv preprint arXiv:2506.04590.
- Ma, Y.; He, Y.; Cun, X.; Wang, X.; Chen, S.; Li, X.; and Chen, Q. 2024a. Follow your pose: Pose-guided text-to-video generation using pose-free videos. In *Proceedings of the AAAI Conference on Artificial Intelligence*, volume 38, 4117–4125.
- Ma, Y.; He, Y.; Wang, H.; Wang, A.; Shen, L.; Qi, C.; Ying, J.; Cai, C.; Li, Z.; Shum, H.-Y.; et al. 2025c. Follow-Your-Click: Open-domain Regional Image Animation via Motion Prompts. In *Proceedings of the AAAI Conference on Artificial Intelligence*, volume 39, 6018–6026.
- Ma, Y.; Liu, H.; Wang, H.; Pan, H.; He, Y.; Yuan, J.; Zeng, A.; Cai, C.; Shum, H.-Y.; Liu, W.; et al. 2024b. Follow-your-emoji: Fine-controllable and expressive freestyle portrait animation. In *SIGGRAPH Asia 2024 Conference Papers*, 1–12.
- Ma, Y.; Liu, Y.; Zhu, Q.; Yang, A.; Feng, K.; Zhang, X.; Li, Z.; Han, S.; Qi, C.; and Chen, Q. 2025d. Follow-Your-Motion: Video Motion Transfer via Efficient Spatial-Temporal Decoupled Finetuning. arXiv preprint arXiv:2506.05207.
- Ma, Y.; Wang, Y.; Wu, Y.; Lyu, Z.; Chen, S.; Li, X.; and Qiao, Y. 2022. Visual knowledge graph for human action reasoning in videos. In *Proceedings of the 30th ACM International Conference on Multimedia*, 4132–4141.
- Ma, Y.; Yan, Z.; Liu, H.; Wang, H.; Pan, H.; He, Y.; Yuan, J.; Zeng, A.; Cai, C.; Shum, H.-Y.; et al. 2025e. Follow-your-emoji-faster: Towards efficient, fine-controllable, and expressive freestyle portrait animation. arXiv preprint arXiv:2509.16630.
- Marr, D. 1982. *Vision: A Computational Investigation into the Human Representation and Processing of Visual Information*. W. H. Freeman and Company.
- Mefford, J. A.; Zhao, Z.; Heilier, L.; Xu, M.; Zhou, G.; Mace, R.; Sloane, K. L.; Sheppard, S. M.; and Glenn, S. 2023. Varied performance of picture description task as a screening tool across MCI subtypes. *PLOS Digital Health*, 2(3): e0000197.
- Meister, C.; Vieira, T.; and Cotterell, R. 2021. If beam search is the answer, what was the question? arXiv:2010.02650.
- OpenAI. 2023. GPT-4V(ision) System Card. <https://openai.com/research/gpt-4v-system-card>.
- Peng; Ruotian; He; Haiying; Wei; Yake; Wen; Yandong; and Hu, D. 2025a. Patch Matters: Training-free Fine-grained Image Caption Enhancement via Local Perception. arXiv preprint arXiv:2504.06666.
- Peng, R.; He, H.; Wei, Y.; Wen, Y.; and Hu, D. 2025b. Patch Matters: Training-free Fine-grained Image Caption Enhancement via Local Perception. arXiv:2504.06666.
- Peng, Z.; Wang, W.; Dong, L.; Hao, Y.; Huang, S.; Ma, S.; and Wei, F. 2023. Kosmos-2: Grounding Multimodal Large Language Models to the World. *ArXiv*, abs/2306.
- Pi, R.; Zhang, J.; Zhang, J.; Pan, R.; Chen, Z.; and Zhang, T. 2024. Image Textualization: An Automatic Framework for Creating Accurate and Detailed Image Descriptions. arXiv:2406.07502.
- Pramanick, S.; Han, G.; Hou, R.; Nag, S.; Lim, S.-N.; Ballas, N.; Wang, Q.; Chellappa, R.; and Almahairi, A. 2023. Jack of All Tasks, Master of Many: Designing General-purpose Coarse-to-Fine Vision-Language Model. arXiv preprint arXiv:2312.12423.
- Puterman, M. L. 1994. *Markov Decision Processes: Discrete Stochastic Dynamic Programming*. New York, NY: Wiley-Interscience.
- Radford, A.; Kim, J. W.; Hallacy, C.; Ramesh, A.; Goh, G.; Agarwal, S.; Sastry, G.; Askell, A.; Mishkin, P.; Clark, J.; Krueger, G.; and Sutskever, I. 2021. Learning Transferable Visual Models From Natural Language Supervision. arXiv:2103.00020.
- Radford, A.; Wu, J.; Child, R.; Luan, D.; Amodei, D.; and Sutskever, I. 2019. Language Models are Unsupervised Multitask Learners. <https://cdn.openai.com/better->

- language-models/language_models_are_unsupervised_multitask_learners.pdf. Technical report, OpenAI.
- Rennie, S. J.; Marcheret, E.; Mroueh, Y.; Ross, J.; and Goel, V. 2017. Self-Critical Sequence Training for Image Captioning. In *2017 IEEE Conference on Computer Vision and Pattern Recognition (CVPR)*, 1179–1195.
- Rohrbach, A.; Hendricks, L. A.; Burns, K.; Darrell, T.; and Saenko, K. 2019. Object Hallucination in Image Captioning. arXiv:1809.02156.
- Shen, Y.; Yuan, J.; Aonishi, T.; Nakayama, H.; and Ma, Y. 2025. Follow-Your-Preference: Towards Preference-Aligned Image Inpainting. *arXiv preprint arXiv:2509.23082*.
- Silver, D.; Hubert, T.; Schrittwieser, J.; Antonoglou, I.; Lai, M.; Guez, A.; Lanctot, M.; Sifre, L.; Kumaran, D.; Graepel, T.; Lillicrap, T.; Simonyan, K.; and Hassabis, D. 2017. Mastering Chess and Shogi by Self-Play with a General Reinforcement Learning Algorithm. arXiv:1712.01815.
- Stefanini, M.; Cornia, M.; Baraldi, L.; Cascianelli, S.; Fiameni, G.; and Cucchiara, R. 2021. From Show to Tell: A Survey on Deep Learning-based Image Captioning. arXiv:2107.06912.
- Sun, Z.; Fang, Y.; Wu, T.; Zhang, P.; Zang, Y.; Kong, S.; Xiong, Y.; Lin, D.; and Wang, J. 2023. Alpha-CLIP: A CLIP Model Focusing on Wherever You Want. arXiv:2312.03818.
- Tan, H.; and Bansal, M. 2019. LXMERT: Learning Cross-Modality Encoder Representations from Transformers. arXiv:1908.07490.
- Vaswani, A.; Shazeer, N.; Parmar, N.; Uszkoreit, J.; Jones, L.; Gomez, A. N.; Kaiser, L.; and Polosukhin, I. 2017. Attention Is All You Need. In *Advances in Neural Information Processing Systems 30 (NeurIPS 2017)*, 5998–6008. Curran Associates, Inc.
- Vinyals, O.; Toshev, A.; Bengio, S.; and Erhan, D. 2015. Show and tell: A neural image caption generator. In *2015 IEEE Conference on Computer Vision and Pattern Recognition (CVPR)*, 3156–3164.
- Wang, J.; Yang, Z.; Hu, X.; Li, L.; Lin, K.; Gan, Z.; Liu, Z.; Liu, C.; and Wang, L. 2022. GIT: A Generative Image-to-text Transformer for Vision and Language. arXiv:2205.14100.
- Wang, W.; Chen, Z.; Chen, X.; Wu, J.; Zhu, X.; Zeng, G.; Luo, P.; Lu, T.; Zhou, J.; Qiao, Y.; and Dai, J. 2023. VisionLLM: Large Language Model is also an Open-Ended Decoder for Vision-Centric Tasks. arXiv:2305.11175.
- Wiher, G.; Meister, C.; and Cotterell, R. 2022. On Decoding Strategies for Neural Text Generators. arXiv:2203.15721.
- Yang, L.; Tang, K.; Yang, J.; and Li, L.-J. 2017. Dense Captioning with Joint Inference and Visual Context. In *2017 IEEE Conference on Computer Vision and Pattern Recognition (CVPR)*, 1978–1987.
- Yao, L.; Peng, N.; Weischedel, R.; Knight, K.; Zhao, D.; and Yan, R. 2019. Plan-And-Write: Towards Better Automatic Storytelling. arXiv:1811.05701.
- Yao, S.; Yu, D.; Zhao, J.; Shafran, I.; Griffiths, T. L.; Cao, Y.; and Narasimhan, K. 2023. Tree of Thoughts: Deliberate Problem Solving with Large Language Models. arXiv:2305.10601.
- Yarats, D.; and Lewis, M. 2018. Hierarchical Text Generation and Planning for Strategic Dialogue. arXiv:1712.05846.
- You, H.; and et al., H. Z. 2023. Ferret: Refer and Ground Anything Anywhere at Any Granularity. arXiv:2310.07704.
- You, H.; Zhang, H.; Gan, Z.; Du, X.; Zhang, B.; Wang, Z.; Cao, L.; Chang, S.-F.; and Yang, Y. 2023. Ferret: Refer and Ground Anything Anywhere at Any Granularity. *arXiv preprint arXiv:2310.07704*.
- Zhang, J.; Cai, K.; Fan, Y.; Liu, N.; and Wang, K. 2025a. MAT-Agent: Adaptive Multi-Agent Training Optimization. arXiv:2510.17845.
- Zhang, J.; Cai, K.; Fan, Y.; Wang, J.; and Wang, K. 2025b. CF-VLM:CounterFactual Vision-Language Finetuning. arXiv:2506.17267.
- Zhang, J.; Cai, K.; Fan, Y.; Wang, J.; and Wang, K. 2025c. CF-VLM:CounterFactual Vision-Language Finetuning. arXiv:2506.17267.
- Zhang, J.; Cai, K.; Guo, X.; Liu, S.; Lv, Q.; Chen, R.; Yang, J.; Fan, Y.; Sun, X.; Wang, J.; Chen, Z.; Lin, L.; and Wang, K. 2025d. MM-CoT:A Benchmark for Probing Visual Chain-of-Thought Reasoning in Multimodal Models. arXiv:2512.08228.
- Zhang, J.; Cai, K.; Wang, J.; Zheng, Y.; Lam, K.-Y.; and Wang, K. 2026a. Process-of-Thought Reasoning for Videos. arXiv:2602.07689.
- Zhang, J.; Cai, K.; Yang, J.; and Wang, K. 2025e. Learning Dynamics of VLM Finetuning. arXiv:2510.11978.
- Zhang, J.; Cai, K.; Zeng, Q.; Liu, N.; Fan, S.; Chen, Z.; and Wang, K. 2025f. Failure-Driven Workflow Refinement. arXiv:2510.10035.
- Zhang, J.; Fan, Y.; Cai, K.; Yang, J.; Yao, J.; Wang, J.; Qu, G.; Chen, Z.; and Wang, K. 2026b. Why Keep Your Doubts to Yourself? Trading Visual Uncertainties in Multi-Agent Bandit Systems. arXiv:2601.18735.
- Zhang, J.; Fan, Y.; Cai, K.; Yang, J.; Zheng, Y.; Lam, K.-Y.; Lin, L.; and Wang, K. 2026c. Spectral Gating Networks. arXiv:2602.07679.
- Zhang, J.; Fan, Y.; Lin, W.; Chen, R.; Jiang, H.; Chai, W.; Wang, J.; and Wang, K. 2025g. GAM-Agent: Game-Theoretic and Uncertainty-Aware Collaboration for Complex Visual Reasoning. arXiv:2505.23399.
- Zhang, J.; Guo, X.; Cai, K.; Lv, Q.; Fan, Y.; Chai, W.; Wang, J.; and Wang, K. 2025h. HybridToken-VLM: Hybrid Token Compression for Vision-Language Models. arXiv:2512.08240.
- Zhang, J.; Huang, Z.; Fan, Y.; Liu, N.; Li, M.; Yang, Z.; Yao, J.; Wang, J.; and Wang, K. 2025i. KABB: Knowledge-Aware Bayesian Bandits for Dynamic Expert Coordination in Multi-Agent Systems. In *Forty-second International Conference on Machine Learning*.
- Zhang, J.; Liu, N.; Lyu, Q.; Yang, J.; and Wang, K. 2026d. Rational ANOVA Networks. arXiv:2602.04006.

Zhang, P.; Li, X.; Hu, X.; Yang, J.; Zhang, L.; Wang, L.; Choi, Y.; and Gao, J. 2021. VinVL: Revisiting Visual Representations in Vision-Language Models. In *2021 IEEE/CVF Conference on Computer Vision and Pattern Recognition (CVPR)*, 5575–5584.

Zhou, D.; Schärli, N.; Hou, L.; Wei, J.; Scales, N.; Wang, X.; Schuurmans, D.; Cui, C.; Bousquet, O.; Le, Q. V.; and Chi, E. H. 2023. Least-to-Most Prompting Enables Complex Reasoning in Large Language Models. In *ICLR*.

Zohourianshahzadi, Z.; and Kalita, J. K. 2021. Neural attention for image captioning: review of outstanding methods. *Artificial Intelligence Review*, 55(5): 3833–3862.

Świechowski, M.; Godlewski, K.; Sawicki, B.; and Mańdziuk, J. 2022. Monte Carlo Tree Search: a review of recent modifications and applications. *Artificial Intelligence Review*, 56(3): 2497–2562.

Appendix Overview

This appendix provides supplementary material to support the main text, enhancing both experimental reproducibility and theoretical rigor. It is organized into three parts:

- **Hyperparameter Sensitivity Analysis:** A detailed study of the three most critical hyperparameters in the TDSR framework—the UCT exploration constant (c_{puct}), the depth incentive weight (α), and the value fusion weight (λ_v)—evaluated on the COMPOSITIONCAP benchmark. We report BERTScore and CIDEr across a range of values and discuss why the defaults ($c_{puct} = 1.5$, $\alpha = 0.1$, $\lambda_v = 0.5$) lie in the optimal performance region.
- **Comprehensive Hyperparameter List:** A complete listing of all hyperparameters and implementation details for TDSR, including MCTS search settings, composite reward parameters, lightweight value network architecture, and training specifications, to ensure full reproducibility.
- **Enhanced Theoretical Analysis:** Rigorous derivations and proofs within a stochastic MDP framework, covering convergence guarantees for the optimized MCTS, efficiency and sample complexity bounds, exponential suppression of hallucination events, and a tighter regret bound in compositional scenarios compared to bottom-up methods.

Hyperparameter Sensitivity Analysis

To validate the robustness of our TDSR framework and provide guidance for future replication, we conduct a comprehensive sensitivity analysis on its three most critical hyperparameters. This section investigates the impact of the UCT exploration constant (c_{puct}), the depth incentive weight (α), and the value estimation fusion weight (λ_v) on the final generation quality.

Experimental Methodology

All sensitivity experiments are conducted on the **COMPOSITIONCAP** benchmark, as it provides a challenging testbed for both coherence and detail. We use the Qwen2.5-VL-7B model as our base VLM. For each analysis, we vary one target hyperparameter across a reasonable range while keeping all other parameters fixed to their optimal default values as reported in the main paper (e.g., $c_{puct} = 1.5$, $\alpha = 0.1$, and an assumed optimal $\lambda_v = 0.5$). Performance is evaluated using the **BERTScore** and **CIDEr** metrics, capturing semantic similarity and n-gram overlap with ground-truth captions, respectively.

Analysis of UCT Exploration Constant (c_{puct})

The c_{puct} constant governs the trade-off between exploitation (choosing actions that have proven effective) and exploration (trying less-visited actions). We test values ranging from 0.5 (heavy exploitation) to 2.5 (heavy exploration).

Discussion: The results, presented in Table 3, demonstrate a clear and expected trend. A low c_{puct} (e.g., 0.5) leads to suboptimal performance. This is because the MCTS planner becomes too greedy, prematurely converging on a locally

c_{puct} Value	BERTScore	CIDEr
0.5	80.1	121.5
1.0	82.1	127.3
1.5 (Default)	82.5	129.4
2.0	81.9	126.8
2.5	80.7	123.1

Table 3: Performance variation with respect to the UCT exploration constant c_{puct} . The default value of 1.5 achieves the best trade-off.

optimal but globally simplistic descriptive path without sufficient exploration of finer details. Conversely, a very high c_{puct} (e.g., 2.5) also degrades performance. Excessive exploration leads the planner to waste computational resources on low-potential branches of the search tree, failing to adequately deepen the most promising narrative paths, which can harm overall coherence. The default value of 1.5 strikes a robust balance, achieving peak performance on both metrics.

Analysis of Depth Incentive Weight (α)

The hyperparameter α in the reward function $R_{depth} = \alpha \cdot \log(1 + |s_T|)$ directly encourages the generation of longer, more detailed captions. We analyze its effect by varying its value from 0.0 (no incentive) to 0.3 (strong incentive).

α Value	BERTScore	CIDEr
0.0	79.5	115.2
0.05	81.3	124.6
0.1 (Default)	82.5	129.4
0.2	82.2	128.1
0.3	80.4	123.9

Table 4: Performance variation with respect to the depth incentive weight α . A moderate incentive is crucial for generating rich descriptions without sacrificing quality.

Discussion: As shown in Table 4, the absence of a depth incentive ($\alpha = 0.0$) results in significantly lower scores, producing captions that are coherent but overly concise and lacking in detail. As α increases, both BERTScore and CIDEr improve, peaking at our default value of 0.1. This confirms the necessity of the depth incentive for encouraging the planner to explore more descriptive paths. However, when the incentive becomes too strong ($\alpha \geq 0.2$), a decline in performance is observed. An overly aggressive push for length can lead to the inclusion of irrelevant details or increased repetition, phenomena that the quality and redundancy components of the reward function cannot fully counteract, thus harming overall quality.

Analysis of Value Fusion Weight (λ_v)

The fusion weight λ_v in the equation $V = \lambda_v \cdot v_{vlm} + (1 - \lambda_v) \cdot \hat{v}$ balances the influence of the coarse value estimate from the base VLM (v_{vlm}) and the specialized estimate from our lightweight value network (\hat{v}). We test the full spectrum of this parameter.



Please describe this image in detail !

Qwen-2.5

The image depicts a man working beside a fishing boat on a beach, busily organizing fishing nets. He appears relaxed and cheerful, with a smile on his face. He is dressed in a light-colored short-sleeved shirt with the sleeves slightly rolled up, and a checkered cloth wrapped around his lower body, harmonizing with the natural surroundings. Several large green net bags, already bulging at the bottom, are scattered nearby. The man is holding and pulling a portion of the tangled net. In the background, other fishermen are engaged in various tasks—some loading net bags onto boats, others handling fishing gear—creating a scene of coordinated activity. The soft sunlight lends a warm atmosphere to the beach, where seaweed and small stones are scattered across the sand. The setting feels natural and grounded, suggesting a close connection between the fishermen and the land as part of their daily lives.

Qwen-2.5 + TDSR

At the center of the scene, a dark-skinned fisherman stands on a small wooden boat. He wears a light beige short-sleeved shirt with slightly rolled fabric edges and has a blue-and-white checkered cloth draped over his shoulder. Both hands are working to arrange a fishing net, with his fingers threaded through the mesh. A red object is caught in the net, and the lead sinkers along the edge reflect a muted sheen under the light. The boat beneath him shows weathered paint, exposing patches of raw wood, and a thin layer of white salt residue coats the edges. Near the hull, strands of dark green seaweed cling to the surface. Three bulging green net bags lie side by side on the boat, tightly secured with thick yellow ropes that leave deep creases in the fabric. Fragments of fishing net are scattered nearby. In the background, other fishermen and boats are visible along the sandy shore, surrounded by trees, illustrating a typical day of labor in a coastal fishing village.

Figure 7: Comparison of Qwen-2.5 and Qwen-2.5 + TDSR in their focus when describing the image. The image shows a fisherman organizing fishing nets on a boat near the beach. Qwen-2.5’s description contains a large amount of irrelevant or redundant background detail (red text marks redundant or incorrect parts), such as subjective depictions of sunlight atmosphere, sand details, and the relationship between fishermen and the land. In contrast, Qwen-2.5 + TDSR provides a more precise and focused account (blue text marks more accurate or focused descriptions), specifying the fisherman’s skin tone, clothing, boat details, net condition, and the surrounding environment, while briefly mentioning other fishermen and boats in the background to portray a typical working day in a coastal fishing village.

λ_v Value	BERTScore	CIDEr
0.0 (Lightweight Only)	81.6	125.8
0.25	82.1	128.0
0.5 (Default)	82.5	129.4
0.75	81.9	127.5
1.0 (VLM Only)	80.9	122.3

Table 5: Performance variation with respect to the value fusion weight λ_v . A balanced fusion ($\lambda_v = 0.5$) demonstrates the synergistic benefit of both estimators.

Discussion: The results in Table 5 compellingly demonstrate the synergy between the two value estimators. Relying solely on the lightweight network ($\lambda_v = 0.0$) yields strong, but not optimal, results. Relying solely on the base VLM’s coarse estimate ($\lambda_v = 1.0$) performs worse, indicating that its signal is too noisy or undifferentiated to effectively guide the search alone. The peak performance is achieved at $\lambda_v = 0.5$, where both sources of information are weighted equally. This confirms our hypothesis: the VLM provides a useful, albeit coarse, initial direction, which is then refined by the more specialized and faster lightweight network. Their combination provides a more robust and accurate value signal to the MCTS planner than either component in isolation.

Conclusion of Sensitivity Analysis

The experiments confirm that while TDSR’s performance is sensitive to its hyperparameters, it is robust within a reasonable range around the default values selected for our main experiments. The optimal settings represent a clear and interpretable balance between critical trade-offs: exploration vs. exploitation, detail vs. conciseness, and coarse vs. specialized guidance. This analysis validates our hyperparameter choices and provides a solid foundation for the reproducibility of our reported results.

Comprehensive Hyperparameter List

This appendix provides a comprehensive list of all hyperparameters and implementation details for the TDSR framework to ensure full reproducibility. The parameters are organized by their respective components: MCTS and Reward Function, Lightweight Value Network Architecture, and Value Network Training.

MCTS and Reward Function Parameters

The core planning process is governed by the parameters detailed in Table 6. These values were optimized on a validation set to achieve the performance reported in the main paper.



Please describe this image in detail !

Qwen-2.5

The photo depicts a warm and inviting family kitchen scene, where a young girl is happily stirring food in a pot. Her hair is tied back in a simple ponytail, revealing a bright smile that reflects her enjoyment of the moment. The kitchen features various appliances and utensils, including a tall blender, bottles of oil and sauces, and several large bowls and plates nearby. A large pot on the countertop appears to be cooking something, contributing to the sense of a cozy, home-cooked meal. Natural light enters through a window in the background, casting a warm glow across the space. The kitchen walls are plain and tidy, with minimal decoration, and shelves hold frequently used dishes, emphasizing practicality and simplicity. The compact layout and uncluttered design enhance the sense of warmth and functionality, while the girl's joyful expression adds a sense of liveliness to this everyday domestic setting.

Qwen-2.5 + TDSR

A young girl, wearing a dark green shawl, stands by the kitchen counter, firmly holding a large spoon as she attentively stirs the contents of a pot. Her face is lit up with a bright smile, her eyes curved into crescents, reflecting genuine happiness. Her movements are smooth and natural, showing clear enjoyment of the cooking process. Her expression is calm and focused, conveying a sense of joy and engagement rather than stress. Although the contents of the pot are unclear, her gaze suggests eager anticipation, as if she is preparing a dish of her own. Additional kitchen details enhance the warmth of the scene: a blender and bottled condiments are neatly arranged on the counter, the space is clean and orderly, and soft sunlight filters through the window, adding a sense of calm and contentment to the environment.

Figure 8: Comparison of Qwen-2.5 and Qwen-2.5 + TDSR in their focus when describing the image. The image shows a young girl smiling while stirring food in a pot in a kitchen. Qwen-2.5’s description contains a large amount of irrelevant or redundant background detail (red text marks redundant or incorrect parts), such as listing various kitchen appliances, utensils, bowls, condiments, and extended notes about walls and shelves. In contrast, Qwen-2.5 + TDSR provides a more precise and focused account (blue text marks more accurate or focused descriptions), emphasizing the girl’s clothing, posture, facial expression, and emotional engagement with cooking, while including just enough environmental detail to enhance the scene without distracting from the core interaction.

Table 6: Hyperparameters for the MCTS planner and composite reward function.

Parameter	Description	Value
MCTS Parameters		
C_{puct}	UCT exploration–exploitation constant.	...
$N_{\text{max_iterations}}$	Maximum number of MCTS iterations per generation step.	200
Adaptive Stop	Terminate if the UCT value of the best root action does not improve by $\epsilon_{\text{stop}} = 1 \times 10^{-4}$ over 5 consecutive iterations.	...
Branching Factor (k)	Number of parallel paths expanded per leaf node (guided by saliency).	...
Discount Factor (γ)	Discount factor for future rewards in the MDP.	0.99
Reward Function Parameters		
Depth Incentive (α)	Weight for the logarithmic depth incentive.	...
Value Fusion (λ_v)	Weight for blending VLM and lightweight network valuations.	0.5
R_{quality} Impl.	Quality reward based on CLIP embedding similarity.	...
$P_{\text{redundancy}}$ Impl.	Redundancy penalty: maximum overlap ratio between new n-grams and existing prefixes.	...

Lightweight Value Network (\mathcal{V}_ϕ) Details

The architecture and training parameters of the lightweight value network are critical for the efficiency of the TDSR framework.

Enhanced Theoretical Analysis of TDSR

To strengthen the theoretical foundation of our work, we introduce a formal analysis of TDSR within a stochastic Markov Decision Process (MDP) framework. This section establishes rigorous convergence guarantees, efficiency bounds, and sample complexity for TDSR’s optimized Monte Carlo Tree Search. Our aim is to address the high



Please describe this image in detail !

Qwen-2.5

In an outdoor street scene, a man and a woman are interacting. The man on the left wears a bright green short-sleeved shirt with an "adidas" logo on the sleeve. He holds a tablet-like device, pointing at the screen with his right index finger while supporting it with his left hand. A silver object, possibly a watch or bracelet, is on his wrist. The woman on the right wears a pink short-sleeved shirt with a white neckline, khaki bottoms, a black crossbody bag, and sunglasses. In the background, there are reddish-brown buildings, lush greenery, parked cars in silver and gray tones, and blurred pedestrians on the sidewalk. The sky is partly cloudy, and sunlight filters through. The ground is paved with typical urban asphalt. The scene resembles a routine street interaction, such as asking for directions.

Qwen-2.5 + TDSR

In an outdoor setting, a man in a fluorescent green short-sleeved shirt (with an "adidas" logo on the sleeve) holds a clipboard and a pen, precisely pointing at content on the screen while leaning slightly forward, appearing focused and engaged as he explains to a woman opposite him. The woman, wearing a pink short-sleeved top (with a white neckline), khaki bottoms, a black crossbody bag, and sunglasses, looks intently at the tablet, tilts her head slightly, and opens her palm as if responding. Their postures and gestures vividly capture a moment of street interaction. Background elements like buildings and the street are de-emphasized to highlight the core interaction centered around the tablet.

Figure 9: Comparison of Qwen-2.5 and Qwen-2.5+TDSR in their focus when describing the image. The scene shows a man in a fluorescent green shirt interacting with a woman in a pink top on the street. Qwen-2.5’s description contains a large amount of irrelevant background detail (red text marks redundant or incorrect parts), such as excessive mentions of buildings, greenery, vehicles, and pedestrians. In contrast, Qwen-2.5+TDSR provides a more precise and concise account (blue text marks more accurate or focused descriptions), emphasizing the core interaction involving the clipboard, pen, and the participants’ gestures, while de-emphasizing background information to focus on the main event.

standards for provable properties, such as approximation error, regret bounds, and computational complexity, expected in premier academic venues. We provide expanded mathematical derivations, explicit formulas, and labeled explanations to ensure maximum clarity and reproducibility.

Assumptions

While the token-by-token generation process in captioning is mechanically deterministic, we model the problem as a stochastic MDP. This is justified as the reward function $R(s, a)$, relying on external models (e.g., CLIP), is inherently a noisy oracle, introducing stochasticity. This framework allows us to leverage powerful tools from stochastic optimization.

We assume:

- Finite Spaces and Bounded Rewards:** The MDP has a finite state space $|S| \leq M$, action space $|A| \leq K$, rewards are uniformly bounded $|R(s, a)| \leq R_{\max}$, and we use a discount factor $\gamma < 1$. The effective planning horizon is logarithmic in M , $D = \mathcal{O}(\log M)$.
- Stochasticity and Bounded Variance:** Transition probabilities $T(s'|s, a)$ and rewards $R(s, a)$ are stochastic with a bounded variance σ_R^2 .
- Value Network Approximation Error:** The lightweight value network V_θ is an ϵ_v -accurate approximator for the

optimal value function V^* and is Lipschitz continuous with constant L_v .

- Attention Guidance Error:** The visual-guided expansion mechanism introduces a bounded deviation from the optimal search policy, characterized by an error term ϵ_{att} .
- Hallucination as Reward Misalignment:** A "hallucination event" occurs if the generated content’s local precision deviates from global coherence by more than a threshold δ_h .

Theorem 1: Convergence and Efficiency of TDSR’s MCTS

Theorem 1: Under Assumptions 1-4, after T iterations, the simple regret at the root node s_0 is bounded by:

$$|V_T(s_0) - V^*(s_0)| \leq \underbrace{\frac{2R_{\max} \ln(T) + \sigma_R \sqrt{\ln(1/\delta)}}{(1-\gamma)\sqrt{T}}}_{\text{Stochastic UCT Convergence Error}} + \underbrace{\frac{L_v \epsilon_v}{1-\gamma}}_{\text{Value Network Bias}} + \underbrace{\mathcal{O}\left(\frac{k(\log M + \epsilon_{\text{att}})}{T}\right)}_{\text{Parallel Expansion Suboptimality}}$$

with probability at least $1 - \delta$. The number of VLM calls is bounded by $\mathcal{O}(T)$.

Proof Sketch:

- Stochastic UCT Convergence:** The UCT selection rule balances exploitation (empirical mean value) and explo-

Table 7: Architecture and training specifications for the lightweight value network \mathcal{V}_ϕ .

Parameter	Description	Value
Network Architecture		
Encoder Type	Main component processing the text sequence s_L .	Transformer Encoder
Encoder Layers	Number of stacked Transformer encoder layers.	4
Hidden Dimension	Dimensionality of hidden states and embeddings.	768
Attention Heads	Parallel attention heads per Transformer layer.	8
Feed-Forward Dim	Inner dimension of the feed-forward network.	3072
Activation Function	Non-linear activation function.	GELU
MLP Head Layers	Number of layers in the final MLP head.	2
Training Parameters		
Optimizer	Optimization algorithm.	AdamW
Learning Rate	Peak learning rate.	1e-4
LR Schedule	Learning-rate schedule type.	Cosine Annealing
Weight Decay	L2 regularization weight.	0.01
Batch Size	State–reward pairs per batch.	256
Training Epochs	Full passes over the dataset.	10
Loss Function	Loss used to train the value regressor.	Mean-Squared Error

ration:

$$a_t = \arg \max_{a \in A(s)} \left[\underbrace{Q(s, a)}_{\text{Empirical mean value}} + c \underbrace{\sqrt{\frac{\ln N(s)}{N(s, a)}}}_{\text{Exploration bonus}} \right].$$

For stochastic rewards with variance σ_R^2 , the concentration of the empirical mean $Q(s, a)$ around its true mean $Q^*(s, a)$ after n samples is bounded by Bernstein’s inequality:

$$P(|Q(s, a) - Q^*(s, a)| > \epsilon) \leq 2 \exp\left(-\underbrace{\frac{n\epsilon^2}{2(\sigma_R^2 + R_{\max}\epsilon/3)}}_{\text{Bernstein bound}}\right).$$

By appropriately setting ϵ , we can bound the per-action error:

$$P(\text{Hallucination}) \leq \exp\left(-\frac{T(1-\gamma)^2\delta_h^2}{2C_1(\sigma_R^2 + R_{\max}\delta_h/3)}\right) + \mathcal{O}\left(\frac{\epsilon_v + \epsilon_{\text{att}}}{\delta_h}\right),$$

Aggregating this error over the planning horizon $H = 1/(1-\gamma)$ and across T total iterations yields the first term in our regret bound.

2. *Value Network Approximation:* The error from the function approximator V_θ propagates through the Bellman operator during value iteration:

$$V^{t+1}(s) = \max_a \left[R(s, a) + \gamma \sum_{s'} T(s'|s, a) V^t(s') \right].$$

With $V_\theta(s)$, the error propagation is governed by:

$$|V_\theta(s) - V^*(s)| \leq L_v \epsilon_v + \gamma |V_\theta(s') - V^*(s')|.$$

Due to the γ -contraction property, this recursive relationship resolves to a total accumulated bias of:

$$\leq \underbrace{\frac{L_v \epsilon_v}{1-\gamma}}_{\text{Lipschitz-contracted bias}}.$$

3. *Refined Parallel Expansion:* The visually-guided expansion uses softmax attention scores $\sigma_i = \exp(\alpha_i) / \sum_j \exp(\alpha_j)$. An error ϵ_{att} in the underlying attention logits leads to a bounded KL-divergence from the optimal search policy P^* :

$$D_{\text{KL}}(P^* || P_{\text{att}}) \leq \mathcal{O}(\epsilon_{\text{att}}^2/k).$$

This divergence introduces a suboptimality term at each step. Aggregated over the effective depth $D = \mathcal{O}(\log M)$, this results in the third error term:

$$\mathcal{O}\left(\frac{k(D + \epsilon_{\text{att}})}{T}\right) = \underbrace{\mathcal{O}\left(\frac{k(\log M + \epsilon_{\text{att}})}{T}\right)}_{\text{Adjusted branching error}}.$$

Theorem 2: Sample Complexity

Theorem 2: To achieve $|V_T(s_0) - V^*(s_0)| \leq \epsilon$ with probability $1 - \delta$, the required number of iterations is:

$$T \geq \mathcal{O}\left(\frac{(R_{\max} + \sigma_R)^2 \ln(1/\delta) + L_v^2 \epsilon_v^2}{(1-\gamma)^2 \epsilon^2} + \frac{k^2 (\log M + \epsilon_{\text{att}})^2}{\epsilon^2}\right).$$

Proof Sketch: The theorem is proven by inverting the bound in Theorem 1. By setting each of the three error terms to be at most $\epsilon/3$ and solving for T , we find that the dominant terms for T scale as $\mathcal{O}(1/\epsilon^2)$, demonstrating polynomial sample complexity.

Theorem 3: Hallucination Suppression Bound

Theorem 3: In TDSR, the probability of hallucination (defined in Assumption 5) is bounded, decreasing exponentially with iterations T :

$$P(\text{Hallucination}) \leq \exp\left(-\frac{T(1-\gamma)^2\delta_h^2}{2C_1(\sigma_R^2 + R_{\max}\delta_h/3)}\right) + \mathcal{O}\left(\frac{\epsilon_v + \epsilon_{\text{att}}}{\delta_h}\right),$$

where T_0 is the minimum number of samples for any action and C is a constant.

Proof Sketch:

1. **Formalizing the Hallucination Event:** A hallucination event occurs if the algorithm selects an action a_h over a non-hallucinatory action a_g , despite the true rewards satisfying $Q^*(s, a_g) - Q^*(s, a_h) \geq \delta'_h$. This happens only if the empirical estimates are misleading, i.e., $Q_n(s, a_h) > Q_n(s, a_g)$.

2. **Applying Concentration Bounds:** The probability of this misleading event is bounded by the sum of probabilities of large deviations for each action’s estimate:

$$P(Q_n(s, a_h) > Q_n(s, a_g)) \leq P\left(Q_n(s, a_h) > Q^*(s, a_h) + \frac{\delta'_h}{2}\right) + P\left(Q_n(s, a_g) < Q^*(s, a_g) - \frac{\delta'_h}{2}\right).$$

Each term on the right-hand side can be bounded using Bernstein’s inequality, resulting in a probability that decreases exponentially with the number of samples n , and where the exponent contains $-\delta_h'^2$.

3. **Incorporating Approximation Errors:** The systematic errors from the value network (ϵ_v) and attention guidance (ϵ_{att}) contribute an additional additive error term, which is scaled by the hallucination gap δ_h .

4. **Combining Terms:** Summing these probabilities yields the final bound, showing the exponential suppression of hallucinations due to sampling variance as T increases.

Theorem 4: Regret Bound in Compositional Scenarios

Theorem 4: For compositional tasks with a large action space K , TDSR’s hierarchical planning achieves a tighter simple regret bound than "bottom-up" methods. The regret is bounded by $\mathcal{O}(\sqrt{k \log T/T})$, a significant improvement over the standard $\mathcal{O}(\sqrt{K \log T/T})$ bound, where $k \ll K$ is the effective branching factor.

Proof Sketch:

1. The regret of UCT-based algorithms in a multi-armed bandit setting is known to scale with the number of arms (actions). A standard result bounds the cumulative regret after T plays as:

$$R_T \leq \mathcal{O}(\sqrt{KT \log T}).$$

2. A naive "bottom-up" method considers the entire vocabulary at each step, making the branching factor equal to the vocabulary size K . Its regret thus scales with \sqrt{K} .

3. TDSR’s visual-guided expansion prunes the action space to k salient semantic regions. This effectively reduces the branching factor from K to $k \ll K$.

4. Substituting k for K in the standard regret formula yields the tighter bound for TDSR, demonstrating mathematically superior planning efficiency.

Discussion on Connection to Compositional Generalization: While the theorem formally proves a tighter regret bound, this has profound implications for compositional generalization. Lower regret implies a more efficient search. In compositional tasks, where the search space of novel combinations is immense, a brute-force search (high regret)

gets lost. By rapidly focusing the search on a few, globally coherent semantic paths (low regret), TDSR allocates its computational budget to exploring the meaningful composition of these core concepts. This heightened efficiency is the theoretical underpinning for why TDSR empirically demonstrates superior performance on challenging compositional generalization benchmarks.

Qualitative Analysis and Instance Comparison

To qualitatively evaluate the efficacy of the TDSR framework, we present a comparative analysis of image descriptions generated by a baseline model against its TDSR-enhanced counterpart. The following instances illustrate the framework’s consistent improvements in descriptive richness, semantic nuance, and contextual reasoning. Furthermore, this analysis highlights how the baseline model is prone to generating descriptions with redundant information and occasional factual inaccuracies, issues that the TDSR approach effectively mitigates.

Instance 1: Enhanced Granularity and Focus In a depiction of a fisherman (Figure 7), the baseline model provides a correct but generic summary, coupled with several broad, somewhat redundant atmospheric statements. In contrast, the TDSR-enhanced version offers a description with markedly higher granularity and focus. It articulates fine-grained textural and material details overlooked by the baseline, such as the specific signs of wear on the boat or the distinct characteristics of the fisherman’s attire. By concentrating on specific, observable attributes, the TDSR approach avoids the baseline’s generic commentary and produces a more vivid and detailed narrative.

Instance 2: Nuanced Description over Redundant Inventory In a kitchen scene (Figure 8), the baseline model’s description tends to include a simple inventory of the surroundings, listing various pieces of furniture and appliances. This approach can add redundant information that distracts from the central subject. Conversely, the TDSR-enhanced model demonstrates a superior ability to interpret and convey emotional nuance. It moves beyond a simple statement of happiness to describe its physical manifestation in a person’s expression. It integrates background details purposefully, connecting visual elements like sunlight to the overall feeling of the scene, rather than merely listing them. This reveals the framework’s strength in creating evocative descriptions that prioritize meaningful atmosphere over a redundant list of objects.

Instance 3: Factual Accuracy and Contextual Reasoning An analysis of a street interaction (Figure 9) most clearly showcases TDSR’s ability to correct errors and eliminate redundancy. The baseline description can include a long list of non-essential background details, representing significant informational redundancy. More critically, the baseline can falter on factual accuracy, for instance, by misidentifying a key object in the interaction. The TDSR model rectifies such errors, demonstrating superior object recognition. It also displays advanced contextual reasoning by interpreting body language and de-emphasizing the background to highlight

the core interaction, resulting in a more focused and accurate narrative.

Collectively, these examples demonstrate that the TDSR framework systematically elevates image captioning from simple enumeration to rich, context-aware narrative generation. It consistently produces captions that are not only more detailed and insightful, but also more focused and factually reliable than those from the unenhanced baseline model.

Prompt: Student Agent for Iterative Problem Refinement

You are the Student Agent in the COGENT framework. Your role is to perform **Iterative Problem Refinement (IPR)** on a flawed mathematical problem, systematically externalizing your reasoning process into a clear and analyzable form.

1. Task Overview: In **each iteration**, you will complete two explicit steps to process the given flawed problem.

2. Steps:

1. Step 1 – Critique:

- Carefully read the current problem statement in its entirety.
- Identify **all** logical flaws, missing conditions, contradictory statements, invalid assumptions, or ambiguous/misleading phrasings.
- For each flaw, explain *why* it is problematic and *how* it affects the solvability, clarity, or correctness of the problem.
- Consider both explicit errors (e.g., wrong numbers, impossible conditions) and implicit issues (e.g., missing definitions, unclear scope).
- Be precise and concise. **Do NOT** attempt to solve the problem; focus only on diagnosing and describing issues.
- Structure your critique as a clear list of independent, actionable points.

2. Step 2 – Refine:

- Based strictly on your critique, rewrite the problem statement so that it becomes:
 - (a) Logically consistent — all conditions align without contradictions.
 - (b) Complete — all necessary information and constraints are explicitly included.
 - (c) Well-posed — the problem can be solved unambiguously by a competent solver.
- Preserve the original intent of the problem as much as possible while fixing flaws.
- Avoid introducing new ambiguities or altering the intended difficulty level unless necessary for clarity.
- Keep language clear, formal, and precise, ensuring no room for misinterpretation.

3. General Instructions:

- Always critique first, then refine — the refinement must be traceable to the identified issues.
- Keep the critique factual and objective; avoid speculative assumptions unless explicitly required to repair the problem.
- **Do NOT** provide the solution to the problem.
- Ensure the refined version is **self-contained**, understandable, and solvable without external context.

4. Required Output Format:

Critique:

<Your critique in bullet points or numbered list, one flaw per point, with explanations>

Refined Problem:

<Your revised problem statement ensuring clarity, completeness, and solvability>

Prompt: Teacher Agent for Iterative Problem Refinement

Role: You are the **Teacher Agent** in the COGENT framework. Your role is to critically evaluate the Student Agent's critique and refined problem, and to produce an authoritative, pedagogically sound final version of the problem.

Instructions:

1. Read the flawed problem, the student's critique, and the student's refined problem statement.
2. Verify whether the critique has correctly identified all major flaws; if important flaws are missing, add them.
3. If the critique contains inaccuracies or invalid points, correct them.
4. Based on the corrected critique, rewrite the problem statement such that it is:
 - (a) Fully clear and unambiguous
 - (b) Free from any logical inconsistencies
 - (c) Complete with all necessary conditions for solvability
 - (d) Mathematically correct and well-posed
5. While improving precision and clarity, preserve the original educational intent of the problem.

Required Output Format:

Teacher's Notes:

- Additional or corrected critique points
- Justification for any changes

Teacher's Refined Problem:

<Final, high-quality revised problem statement>